Yiping Shao
State Key Laboratory of Mechanical System and Vibration, Shanghai Jiao Tong University, Shanghai 200240, China;
School of Mechanical Engineering, Shanghai Jiao Tong University, No. 800 Dongchuan Road, Shanghai 200240, China
e-mail: syp123gh@sjtu.edu.cn

Yaxiang Yin
School of Mechanical Engineering, Shanghai Jiao Tong University, No. 800 Dongchuan Road, Shanghai 200240, China
e-mail: yaxiang@sjtu.edu.cn

Shichang Du[1]
State Key Laboratory of Mechanical System and Vibration, Shanghai Jiao Tong University, Shanghai 200240, China;
School of Mechanical Engineering, Shanghai Jiao Tong University, No. 800 Dongchuan Road, Shanghai 200240, China
e-mail: lovbin@sjtu.edu.cn

Tangbin Xia
Mem. ASME
State Key Laboratory of Mechanical System and Vibration, Shanghai Jiao Tong University, Shanghai 200240, China;
School of Mechanical Engineering, Shanghai Jiao Tong University, No. 800 Dongchuan Road, Shanghai 200240, China
e-mail: xtbxtb@sjtu.edu.cn

Lifeng Xi
State Key Laboratory of Mechanical System and Vibration, Shanghai Jiao Tong University, Shanghai 200240, China;
School of Mechanical Engineering, Shanghai Jiao Tong University, No. 800 Dongchuan Road, Shanghai 200240, China
e-mail: lfxi@sjtu.edu.cn

Leakage Monitoring in Static Sealing Interface Based on Three Dimensional Surface Topography Indicator

Leakage directly affects the functional behavior of a product in engineering practice, and surface topography is one of the main factors in static seal to prevent leakage. This paper aims at monitoring the leakage in static sealing interface, using three-dimensional (3D) surface topography as an indicator. The 3D surface is measured by a high definition metrology (HDM) instrument that can generate millions of data points representing the entire surface. The monitoring approach proposes a series of novel surface leakage parameters including virtual gasket, contact area percentage (CAP), void volume (VV), and relative void volume (SWvoid) as indicators. An individual control chart is adopted to monitor the leakage surface of the successive machining process. Meantime, based on the Persson contact mechanics and percolation theory, the threshold of leakage parameter is found using finite element modeling (FEM). Experimental results indicate that the proposed monitoring method is valid to precontrol the machining process and prevent leakage occurring. [DOI: 10.1115/1.4040620]

Keywords: leakage monitoring, static sealing, three-dimensional surface topography

1 Introduction

Leakage is an important issue of concern in manufacturing industry. When the leakage occurs, it is a huge danger which can cause resources waste, product quality decline, equipment damage, and environment pollution, thereby brings safety accidents and economic losses. Therefore, sealing technology is developed to prevent leakage. A seal is a widely used device for closing a gap and making a joint tight [1]. In many engineering fields, seals play a crucial role to achieve quality and reliability. There are two types of seals: static seal and dynamic seal. Static seal is performed by direct surface to surface contact. Comparing with dynamic seal, static seal is more common in engineering. Direct contact, rubber, and gasket seal are three seal forms corresponding to the seal requirement from low to high, respectively. However, a large number of practices have proved that the leakage still exists with the seals in some industrial applications. Therefore, identifying the leakage mechanism and developing the leakage monitoring approach are essential to precontrol the machining process and ensure the product quality in satisfactory condition and reduce the losses.

Numerous studies were conducted in order to understand sealing and especially leakage. Persson and Yang [2] had proposed a critical-junction theory of the leak-rate of seals, which was based

[1]Corresponding author.
Manuscript received November 15, 2017; final manuscript received June 12, 2018; published online July 9, 2018. Assoc. Editor: Laine Mears.

on percolation theory [3] and Persson contact theory [4]. Soon afterward, the critical-junction theory was verified effectively by a series of researches containing theory comparison and experiment investigation [5,6]. Bottiglione et al. presented a theoretical approach to estimate the fluid leakage mechanism in flat seals by making use of percolation theory and theory of contact mechanics [7,8]. Marie and Lasseux described an experiment study to characterize fluid leakage through a rough metal contact [9]. From these studies, it is clear that the contact pressure, surface topography and the material property of sealing element are three main factors in static seal. Clearly, contact pressure and sealing element are easy to be controlled, but the full control of surface topography during the manufacturing processes is still out of reach. With the limitation of surface characterization and measurement technology, a thorough characterization of surface topography which impacts on the contact efficiency and leakage paths generation are still at the beginning. Therefore, the performance of surface topography on the rate of leakage through seals is the focus of researches among these features.

Due to the existence of roughness and multiscale on surface, it is not a simple matter to know the impact of surface topography on leakage in detail. Waviness motifs-based model was proposed by Robbe-Valloire and Prat to reveal that both the amplitude and the valley to the peak distribution of surface were influential [10]. Okada et al. investigated the quantitative effect of surface profiles on leakage using surface activated bonding technique [11]. Haruyama et al. developed a metal gasket model with different surface roughness levels to evaluate the sealing performance through simulation study [12]. Based on experimental observations, Marie et al. proved that surface components at the intermediate scale, which is corresponding to waviness, was of major concern for leakage [9,13]. In their further study, the modal content of surface components was employed to explore the role on leakage of static flat seal [14]. All these studies indicate the direct relationship between surface topography and leakage, thus surface topography can be considered as an indicator for leakage monitoring.

In general, the vast majority of leakage is detected with a whole part by leak testing machine in the last manufacturing process of production line, and a large number of leakage problems appear during the using of the product. Consequently, it is essential to develop the precontrol measures and leakage monitoring methods. Since the complex leakage mechanism and inconvenient measurement, the leakage monitoring research is less. As a pioneer, Malburg first studied the relationships between the two-dimensional (2D) surface topography and the sealing performance. It is one of the important approaches to investigate the sealing problem and leakage monitoring. Malburg adopted the two-dimensional surface waviness profile parameters to monitor the sealing performance based on a morphological closing filter [15]. Liao et al. pointed the presence of significant middle wavelengths (waviness) would result in leakage, and the tooling marks with the large peak-to-peak variation on the surface were considered as the leakage path [16]. From the data-driven point, Ren et al. first proposed a novel method of modeling and diagnosis of leak areas for surface assembly. A lattice graph model and a color tracking approach were developed to predict potential leak areas and paths in between assembled surfaces [17]. Arghavani et al. proposed a fuzzy logic model to predict the sealing performance and leakage rate of gasketed flange joints using inputs including surface roughness and gas pressure [18]. Xin and Gaoliang presented a leakage prediction calculation method for static seal rings in underground equipment [19]. However, these studies neither explain the surface parameters indicator from the leakage mechanism, nor give the threshold when leakage occurs. Nevertheless, surface topography is still the most suitable indicator, which can provide reliable and detectable information for leakage monitoring.

Recently, an advancement of noncontact laser holographic interferometry measurement, called high definition metrology (HDM), which can generate a surface height map of millions of data points within seconds for three-dimensional (3D) inspection of an entire surface has been developed [20]. Figure 1 shows an engine block surface measured by HDM, there is about 0.8×10^6 data points generated to cover an area of 320 mm × 160 mm with 150 μm lateral resolution in x–y direction and 1 μm accuracy in z direction. With the precision measurement, a preprocessing method is used to convert the mass data points into a height-encoded and position-maintained gray image to represent the entire surface [21]. The 3D surface topography of the entire surface examined by HDM presents a novel platform, several researches based on HDM such as 3D surface topography evaluation [21,22], filtering [23–25], classification [26,27], forecasting [28] and tool wear monitoring methods [29] have been explored for the precontrol of the manufacturing process.

In the meantime, the full and precision measurement also makes it more possible to monitor leakage condition using 3D surface topography indicator. Malburg pointed out that the surface components including form and roughness could be tolerated, but the presence of waviness was highly significant in the static sealing interface. The relationship between surface waviness profile and leakage potential was qualitatively described by several numerical parameters. However, the research only focuses on two-dimensional surface topography and it lacks quantitative analytical information. Meanwhile, the explanation of the relationship between surface parameters and leakage mechanism is absent.

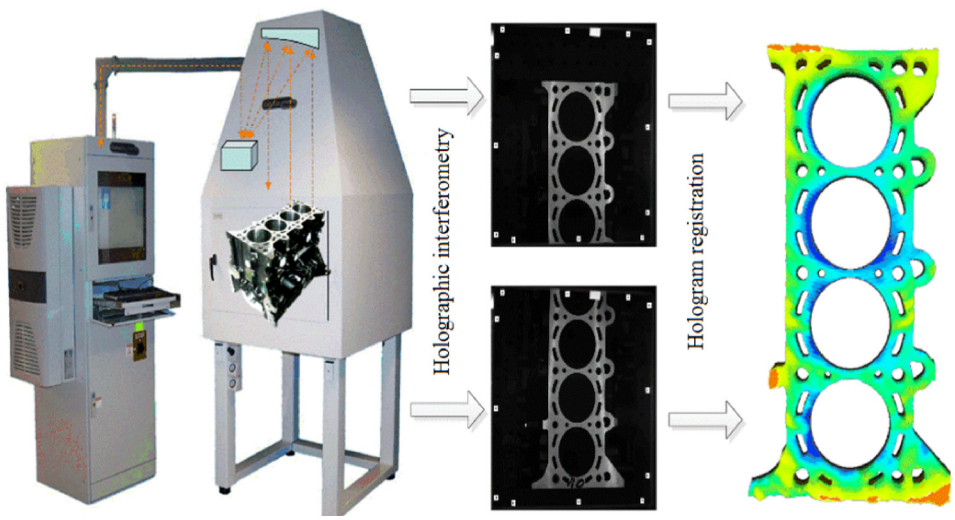

Fig. 1 Measurement by HDM

Therefore, benefitting from the development of measurement, the research focus is extended from two-dimensional surface topography to three-dimensional surface topography. The main contribution of this paper is to present a new leakage monitoring approach using 3D surface topography indicator based on some conclusions of Malburg's research [15].

- The measured surfaces are first separated into different frequency components including form, waviness, and roughness using spline filter. Then, a virtual gasket is generated by the morphological filtering on the waviness.
- A series of novel surface leakage parameters, which including contact area percentage (CAP), void volume (VV), and relative void volume (SWvoid), are defined as indicators for the characteristics of the leakage.
- Meantime, based on the Persson contact mechanics and percolation theory [2–4], the threshold of leakage parameter is found using finite element modeling (FEM).
- Finally, a classical control chart is adopted to monitor the leakage surface of the successive machining process. Results of the engineering case indicate that the proposed monitoring method is valid to precontrol the machining process and prevent leakage occurring.

The paper is organized as follows: a detailed description of leakage monitoring approach is presented in Sec. 2. Then, in Sec. 3, a case study demonstrates the effectiveness of the proposed method. The results illustrate the performance of the proposed approach for leakage monitoring. Finally, the last section draws the conclusions and discusses the future research.

2 The Proposed Method

This section describes an overview of the proposed approach. It consists of surface components extraction, virtual gasket generation, leakage parameters definition and threshold determination and leakage condition monitoring. The framework is shown in Fig. 2. The procedure involves the following steps:

Step 1: Surface components extraction. HDM is employed to measure the engineering surface and generate millions of points. A converted gray image which can represent the entire surface is gained by the points cloud [21]. Then, the high resolution measured surface is filtered to extract form, waviness, and roughness using spline filter [30], which is the ISO accepted linear filter.

Step 2: Virtual gasket generation. A novel concept called virtual gasket is proposed to simulate the actual situation of contact and deformation. The 2D and 3D virtual gasket are generated by 2D and 3D morphological-closing filter based on the waviness profile and surface, respectively.

Step 3: Leakage parameters definition. Three areal leakage parameters CAP, VV, and SWvoid are defined to represent the characteristics of the leakage.

Step 4: Threshold determination and monitoring the leakage condition of the successive machining process. The threshold of leakage parameters is used to determine whether the leakage occurs or not. Based on the Persson contact mechanics and percolation theory, the threshold of leakage parameter is found using FEM analysis. If the value of leakage parameter of a surface region goes beyond the threshold, this surface region is out of limit (OOL), corresponding to leakage area. Subsequently, an individual control chart is used to clearly monitor the leakage conditions of the successive machining process.

2.1 Surface Components Extraction. Surface topography has profound influences on part quality as it plays two vital roles: one is to control the manufacturing process and the other is to help functional prediction. In order to clarify the effect mechanism, filtration is mainly employed in surface metrology, which has been clearly described and specified in ISO 16610-1 [31]. Generally, there are two filters systems: M-system (linear and robust filters) and E-system (morphological and segmentation filters). As a popular linear filter, spline filter has been proved that it can extract and separate surface components exactly. Comparing with classical Gaussian filter, spline filter incorporates improved "form following" capabilities and reduces much boundary effect, which mean that it can be used as a good surface filter for feature extraction.

Spline filter is originally proposed by Krystek [32] and incorporated into ISO 16610-22 [30] as a modified solution to overcome edge distortion and poor performance of large form which are associated with the Gaussian filter. Different from Gaussian filter, filter equation is used instead of the weighting functions to describe spline filter

$$[\mathbf{I} + \beta\alpha^2\mathbf{P} + (1-\beta)\alpha^4\mathbf{Q}]\mathbf{W} = \mathbf{Z} \tag{1}$$

where $\mathbf{I}$ is an $n \times n$ identity matrix, $\mathbf{P}$ is an $n \times n$ tridiagonal symmetric matrix, and $\mathbf{Q}$ is an $n \times n$ five-diagonal symmetric matrix. $\mathbf{Z}$ is the vector of the original data and $\mathbf{W}$ is the vector of the filtered data. $\alpha = 1/(2\sin(\pi\Delta x/\lambda_c))$ and β are the tension parameter which lies between 0 and 1. Δx is the sampling interval and λ_c is the cutoff wavelengths. The recommended value of λ_c can be found in ISO 16610-22 [30], such as 2.5 μm, 8 μm, 25 μm, 80 μm, 250 μm, 0.8 mm, 2.5 mm, 8 mm, 25 mm, and so on. Based on these, waviness profile can be separated from the original profile exactly and Fig. 3 shows a clear illustration.

As an extension of the profile spline, areal spline filter has been implemented and widely used by researchers although the document with ISO 16610-62 has not yet been published. Figure 4 gives an example.

2.2 Virtual Gasket Generation. Morphological filter is more suitable for functional prediction than linear filter, as the logic of the former is more related with the geometrical properties of surfaces. It plays an essential role in understanding static seal interfaces as the various wavelength domains affect the leakage in different ways. Morphological filters were first presented by Magaros and Schafer under the framework of mathematical morphology in 1987 [33], and subsequently they were developed as powerful image processing tools for pattern recognition purposes in various engineering applications. Morphological filters are nonlinear signal transformations that locally modify geometric features of the signal, and they have been accepted in ISO 16610-40 as a part of standard filtration techniques [34].

The natural concept of morphological filter is to perform morphological operations on the surface with structuring elements. There are four basic operations: erosion, dilation, opening, and closing which are listed as follows:

Erosion

$$(f \ominus g^s)(x) = \inf_{y \in D \cap G}\{f(y) - g(y-x)\} \tag{2}$$

Dilation

$$(f \oplus g^s)(x) = \sup_{y \in D \cap G}\{f(y) + g(y-x)\} \tag{3}$$

Opening

$$f \circ g(x) = [(f \ominus g^s) \oplus g](x) \tag{4}$$

Closing

$$f \bullet g(x) = [(f \oplus g^s) \ominus g](x) \tag{5}$$

where the input surface function $f(x)$ and structuring element $g(x)$ are defined in $D \subset \mathbf{R}^n$ and $G \subset \mathbf{R}^n$, respectively, and $g^s(x) = g(-x)$. The erosion operation decreases the peaks and expands the minima of $f(x)$, while the dilation operation gains the opposite result. The opening and closing operations are both used

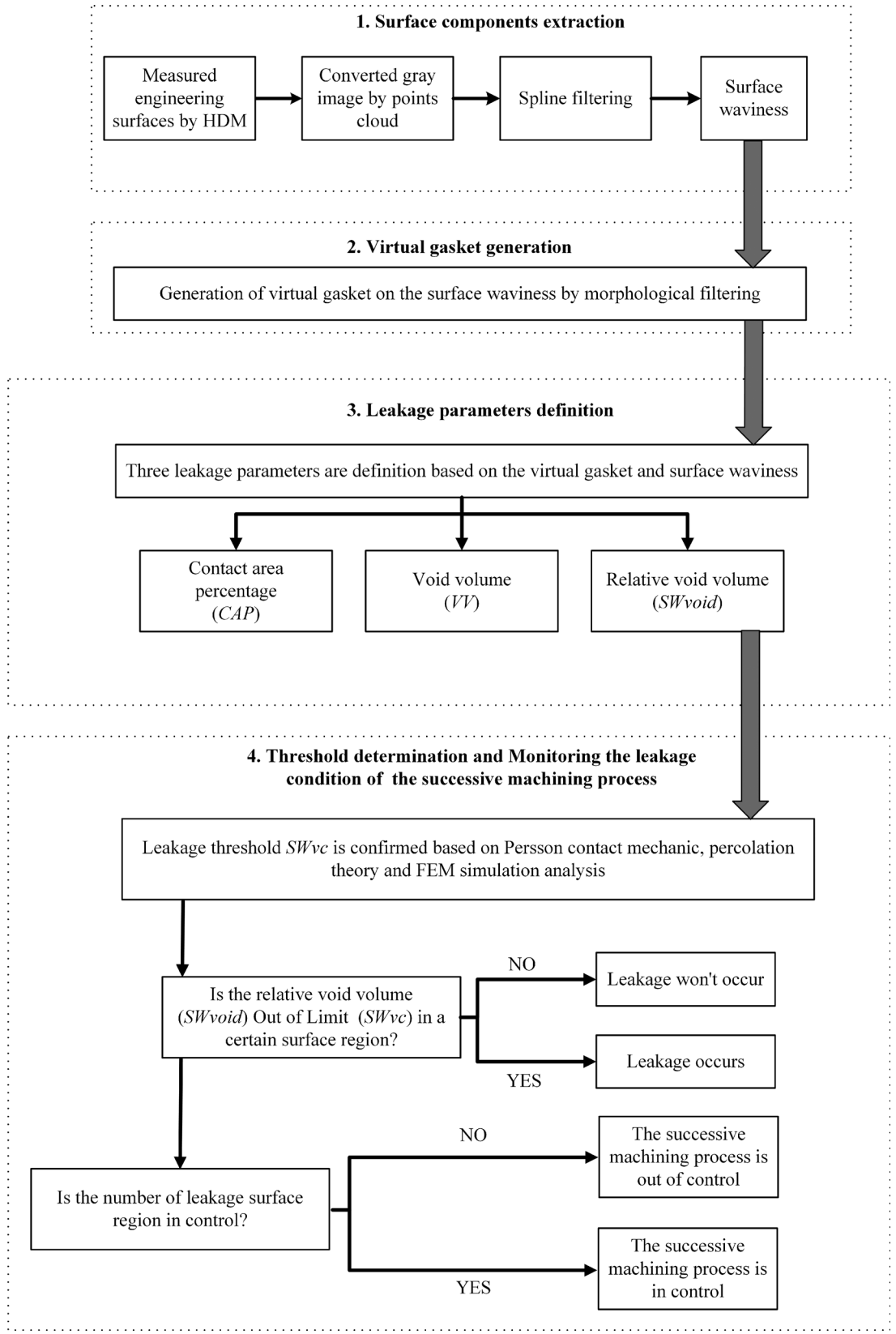

Fig. 2 The framework of the proposed approach

to smooth $f(x)$, the former one is cutting down its peaks from below, and the other is filling up its valleys form above. According to the monotone increasing and idempotence of opening and closing operations, there are two kinds of morphological filters, namely, opening filter and closing filter in geometrical product specifications [34].

Structuring element $g(x)$ is another sticking factor affecting the results of morphological filter. Various kinds of structuring

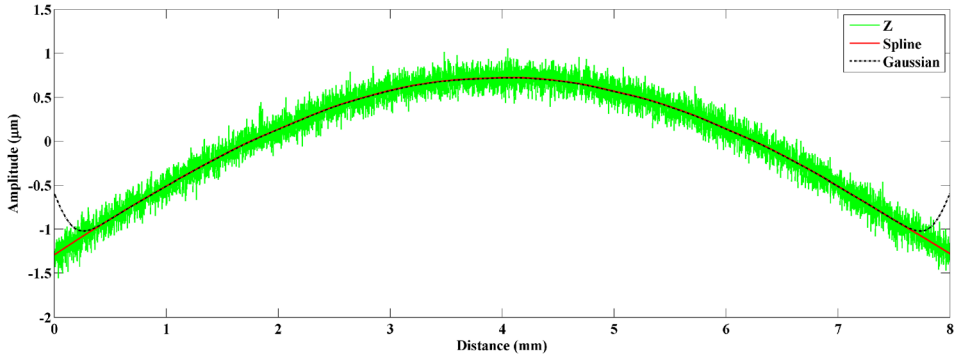

Fig. 3 Profile spline filtering

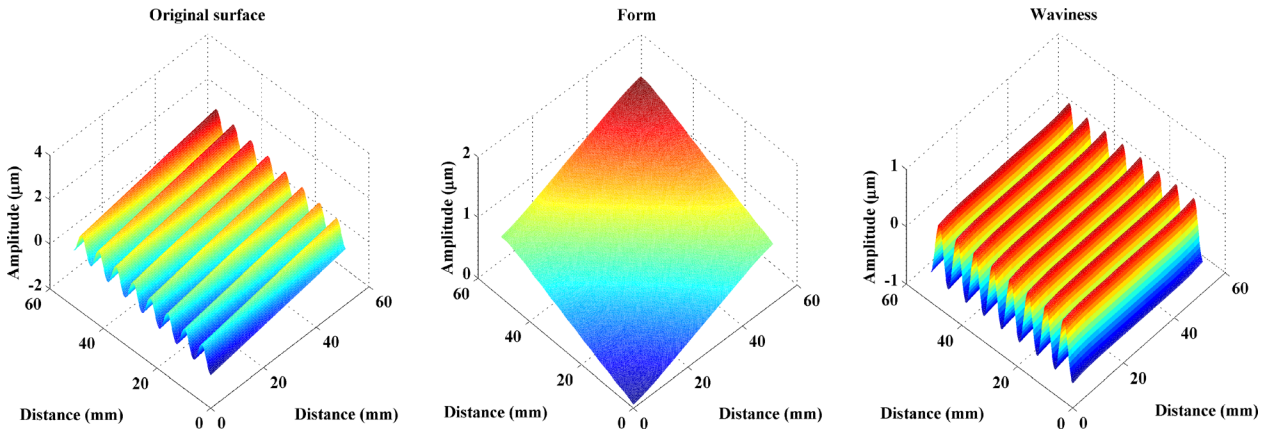

Fig. 4 Areal spline filtering

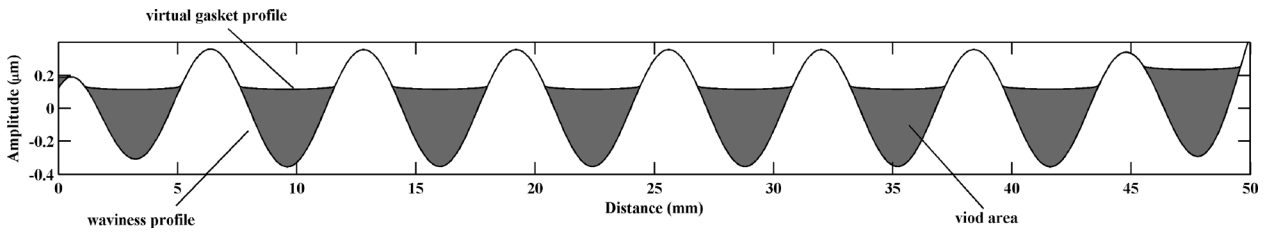

Fig. 5 Virtual gasket profile

elements have been proposed, whereby circular and horizontal line segments for profile and spherical and horizontal planar segments for surface are recommended by ISO 16610-41 and 16610-85 [35,36]. According to the Malburg's research [15], the circular structuring element is chosen to process the engineering surface profile, which is the better one based on its joint properties on the surface profile component. So in this research, spherical structuring element is employed as an extension for areal surface. Moreover, the radius of the structuring element is equally important to the filter results. Considering the actual part's compressive properties (i.e., its ability to "fill gaps") as well as its bending properties, the radius can be confirmed from the recommended values 1 μm, 2 μm, 5 μm, 10 μm, 20 μm, 50 μm, 100 μm, 200 μm, 500 μm, 1 mm, 2 mm, 5 mm, and so on [35].

As the above mentioned, gasket is one of the main seal forms to prevent leakage. To some extent, a gasket can conform to the surface when sealing a surface. Given this property of the gasket, it makes more sense to take note of the gaps between the gasket and the surface features than the peak-to-valley height of the surface. However, due to the limits of measurement, it is difficult and inconvenient to get the real gasket topography and the deformation is unknown in practice. Thus, a new concept named virtual gasket is proposed to simulate the actual situation of contact and deformation. The virtual gasket is derived from the result of a morphological-closing filter, which is similar to rolling a disk over the waviness profile or a ball over the waviness surface. As shown in Figs. 5 and 6, virtual gaskets for profile and surface are generated, respectively in 2D view and 3D view.

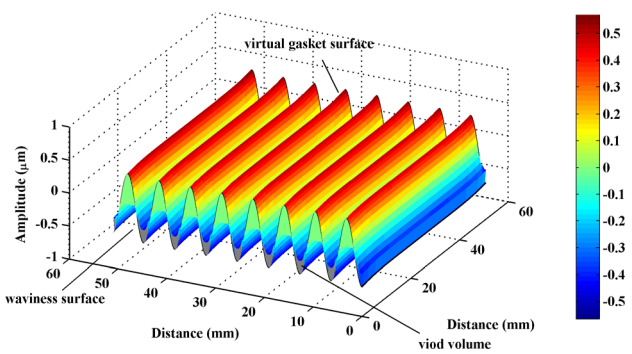

Fig. 6 Virtual gasket surface

2.3 Leakage Parameters Definition. Once the virtual gasket is determined, the next critical process is to quantitatively describe the difference between the virtual gasket and the underlying waviness, which is related to leakage. Malburg first formulated the surface leakage potential by using several numerical parameters, such as contact length percentage (CLP) and void area (VA). The contact length percentage, is the ratio of the number of contact points between the virtual gasket profile $C(x)$ and waviness profile $W(x)$ to the total number of points, which can be used to assess the load distribution. The void area is the enclosed area between the virtual gasket profile $C(x)$ and waviness profile $W(x)$. It is considered as the related area that may lead to leakage. To be specific, the profile leakage parameters are defined as

$$\mathrm{CLP} = \sum_{l} [\text{if } (C_i(x) = W_i(x)) 1 \text{ else } 0]/l \tag{6}$$

$$\mathrm{VA} = \int_0^l (C(x) - W(x))dx \tag{7}$$

where l is the nominal length of surface profile. It is noted that CLP and VA are relied upon the length l, which are not flexible. So the normalized parameter relative void area Wvoid is preferred to describe a void area per unit length, and it is given by the following equation:

$$\mathrm{Wvoid} = \mathrm{VA}/l \tag{8}$$

Benefitting from the development of surface metrology, areal surface parameters have been fully described in ISO 25178-2 [37]. Following the expansion mode of areal surface parameters, an attempt is made to extend the application from 2D surface profile to 3D surface topography, as well as the corresponding areal leakage parameters CAP, VV, and SWvoid. Likewise, with respect to virtual gasket surface $\mathrm{SC}(x, y)$ and waviness surface $\mathrm{SW}(x, y)$, the areal leakage parameters are defined as

$$\mathrm{CAP} = \sum_{S} [\text{if } (\mathrm{SC}_i(x, y) = \mathrm{SW}_i(x, y)) 1 \text{ else } 0]/S \tag{9}$$

$$\mathrm{VV} = \iint_S (\mathrm{SC}(x, y) - \mathrm{SW}(x, y))dxdy \tag{10}$$

$$\mathrm{SWvoid} = \mathrm{VV}/S \tag{11}$$

where S is the nominal area of surface topography. Analogously, CAP and VV are relied upon the nominal area S, which are neither flexible. However, the normalized parameter SWvoid is independent with the area of the surface, which is preferred to describe a void area per unit length clearly. Therefore, SWvoid is first selected to as the leakage indicator to report the leakage area.

With regard to leakage, traditional surface height parameters [37,38] like W_a (mean height of waviness profile), W_t (total height of waviness profile), S_a (mean height of waviness surface) and S_z (maximum height of waviness surface) cannot determine whether the leakage occurs or not effectively. The following waviness profiles, as shown in Fig. 7, have almost the same W_a and W_t, but the generated virtual gaskets are totally different. Obviously, the leakage parameter Wvoid which reports the leakage area can clearly distinguish them. Analogously, the similar performance of 3D surface by SWvoid is graphically depicted in Fig. 8.

2.4 Threshold Determination and Monitoring the Leakage Condition of the Successive Machining Process

2.4.1 Threshold Determination. Based on the proposed leakage parameter (SWvoid), the key problem of leakage monitoring is to find out the threshold of it, which can be named as SWvc. The threshold means a limit of leakage, when the value of SWvoid in a surface region goes beyond SWvc, it can be considered as a leakage region. That is to say, this region is OOL area on this surface, where the leakage occurs probably. It is noted that the threshold is primarily up to the natural attributes of the part and operating condition, such as material and pressure. As a pioneer on leakage mechanism research, Persson et al. had published a series of research including contact mechanics, leak-rate theory, and the factors affecting leakage. Percolation threshold was first proposed to be regard as a flag of the occurrence of leakage [4]. Subsequently, the critical-junction theory was extended to present the quantitative relationship [2].

Assume that the nominal contact region between the gasket and the counter surface is rectangular with area $\mathrm{Lx} \times Ly$(see Fig. 9, the black color means total contact). The high pressure fluid and low pressure fluid are in $x < 0$ region and $x > \mathrm{Lx}$ region, respectively. Furthermore, assume that number $N = Ly/\mathrm{Lx}$, side $\mathrm{Lx} = L$ and area $A_0 = L^2$, N is an integer which does not affect the final results.

In order to understand easily, the study focuses on the contact between the two surfaces within one of the squares as changing the magnification ζ. The magnification ζ is defined as $\zeta = L/\lambda$, where λ is the resolution corresponding to surface scale. As is shown in Fig. 10, the apparent contact area $A(\zeta)$ between the two surfaces is widely divergent with different magnification ζ, and the relative contact area $\mathrm{RC}(\zeta) = A(\zeta)/A_0$. Depending on whether the two surfaces contact or not, each square of the lattice which represents the contact area can be black or white (The black means total contact and the white means no contact). When magnification $\zeta = 1$, any surface roughness cannot be observed and the contact appears to be complete, that is $\mathrm{RC}(\zeta) = 1, A(1) = A_0$. As the magnification ζ increasing, some interfacial roughness appears and the apparent contact area $A(\zeta)$ accordingly decreases. Once magnification ζ is high enough, say $\zeta = \zeta_c$, a percolating channel of noncontact area is eventually formed and leakage occurs (see Fig. 10(*c*)). Instead of determining the critical magnification ζ_c, the relative contact area at this point is given by site percolation theory. Thus, the percolation probability $P(\zeta) = 1 - \mathrm{RC}(\zeta) = 1 - A(\zeta)/A_0$ can directly reflect the relative contact area, and the corresponding $P_c = P(\zeta_c) = 1 - \mathrm{RC}(\zeta_c) = 1 - A(\zeta_c)/A_0$, where P_c is the so called percolation threshold [3].

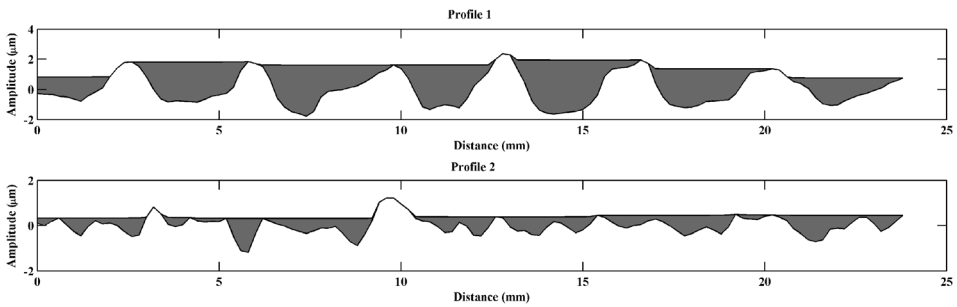

Fig. 7 Different void areas

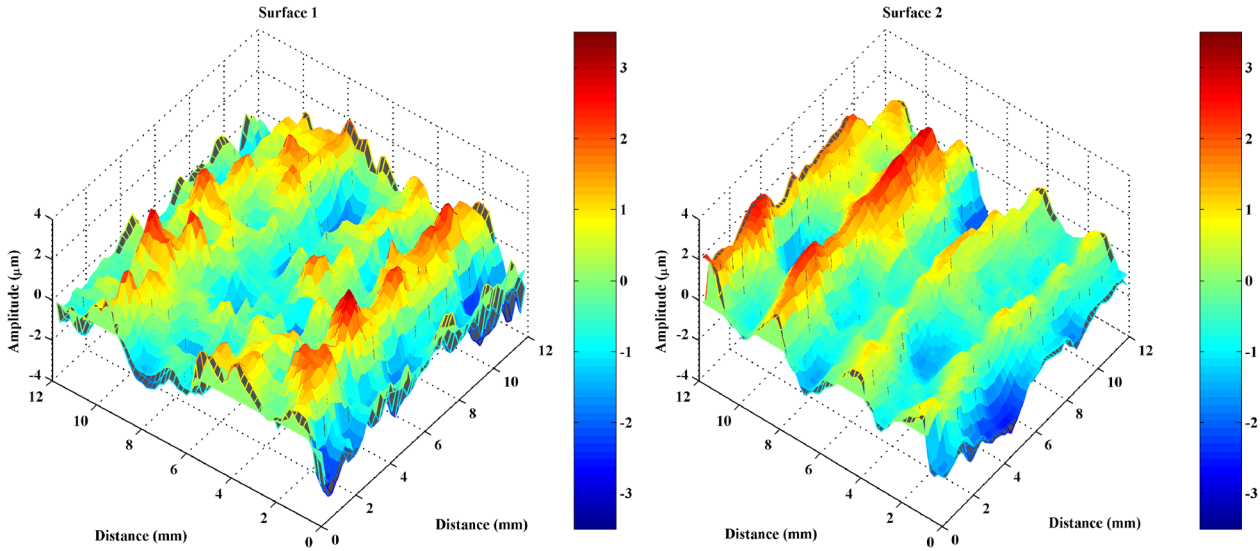

Fig. 8 Different void volumes

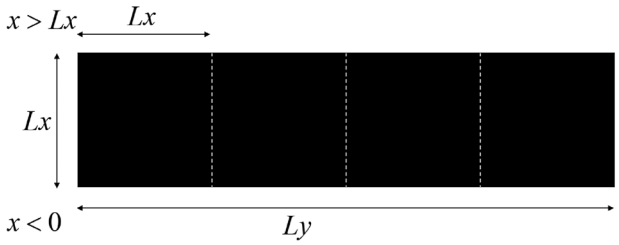

Fig. 9 Contact region

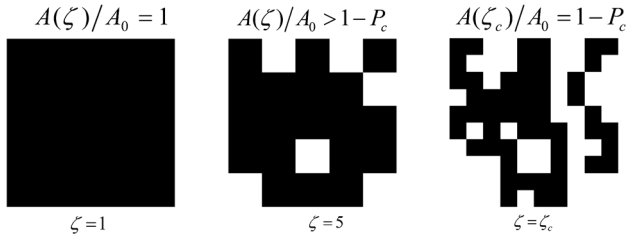

Fig. 10 Evolution of the apparent contact area (The black means total contact and the white means no contact)

For infinite-sized systems, the percolation threshold P_c is about 0.593 for a square lattice and 0.696 for a hexagonal lattice [3]. For finite-sized systems, the percolation threshold will fluctuate between different realizations of the same physical system. Through molecular dynamics results and experimental verification, Persson and Yang [2] pointed that when two elastic solids with randomly rough surfaces were squeezed together, as a function of increasing magnification or decreasing squeezing pressure, a noncontact channel would percolate when the relative contact area $\mathrm{RC}(\zeta_c)$ was of the order 0.4, in accordance with percolation theory. That is to say, when it meets the condition of $P_c \approx 0.6$, $\mathrm{RC}(\zeta_c) = A(\zeta_c)/A_0 \approx 0.4$, leakage occurs.

So, based on the Persson' conclusion, the threshold SWvc of SWvoid can be confirmed by the relative contact area $\mathrm{RC}(\zeta_c) \approx 0.4$ under a certain pressure. Traditionally, the solutions of rough surface contact can be classified into three categories: statistical model, multi-asperity contact model, and deterministic contact model. Many works have shown that there is little difference among the three models, but the former two need more prior knowledge such as the distribution and geometry of asperities, which are not easy to obtain. Fortunately, the deterministic model is based on the directly measured surface data, which reserves the surface geometry as complete as possible. Finite element analysis is a representative and widely used tool in solving deterministic model of rough surface contact [39,40]. Hence, the relative contact area is obtained by finite element model in case study section, and the threshold SWvc can be confirmed subsequently. But determining the value of RC depends on the results of finite element model which is very time-consuming and is not suitable for engineering practice applications. In order to meet the takt time requirement in the practice applications, SWvoid can be easily calculated and used as the leakage indicator.

2.4.2 Monitoring the Leakage Condition of the Successive Machining Process. Generally, leakage is easily caused by the poorly machined parts, but it can be detected only during later product assembly and the costly and wasteful pressure testing, so that it does not prevent additional parts from being poorly machined. Hence, it is possible to develop the monitoring methods of leakage potential prior to product assembly so as to avoid wasted costs, decrease scrap, and enable quick adjustment and control of the machining process before the additional cost of product assembly is incurred.

With a large amount of statistical quality control applications appearing in the industrial field, control chart is a powerful tool for on-line process monitoring or surveillance. The control chart is a device for describing in a precise manner what is meant by statistical control. That is, sample data is collected and used to construct the control chart, and if the sample values fall within the control limits and do not exhibit any systematic pattern, then the process is in control at the level indicated by the chart. To some extent, a surface which exists the leakage is considered as a defective or nonconforming product. Therefore, in monitoring phase, the individual control chart is used to monitor the successive machining process.

As mentioned above, when the leakage parameter SWvoid in a surface region goes beyond the threshold SWvc, this region is OOL area on this surface, namely a leakage region. Assume that n regions are selected in a surface, and the SWvoid of these regions is calculated as $\mathrm{SWvoid}_i (i = 1, \ldots, n)$. Once the parameters SWvoid_i and SWvc are collected, the number of OOL c is defined as

$$c = \sum_{i=1}^{n} k_i \tag{12}$$

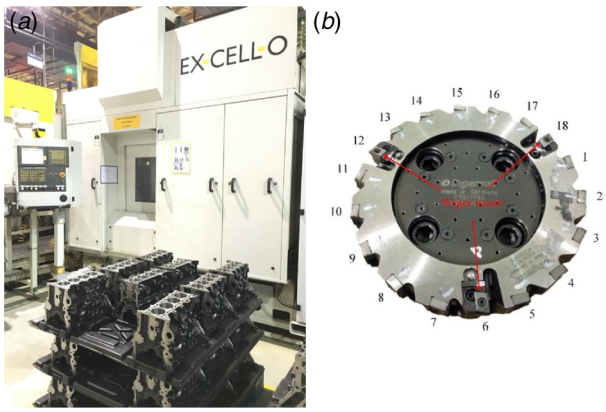

Fig. 11 (*a*) EX-CELL-O machining center and (*b*) the face milling cutter

$$k_i = \begin{cases} 1 & \text{SWvoid}_i \geq \text{SWvc} \\ 0 & \text{SWvoid}_i < \text{SWvc} \end{cases}, \quad i = 1, 2, \ldots, n \tag{13}$$

Suppose that m successive machined surfaces are measured and handled by the above procedures, and the numbers of OOL regions of these surface are obtained as $c_1, c_2, \ldots c_m$. The number of OOL c is the control variable. The centerline, the upper control limit, and the lower control limit (LCL) of the individual chart for leakage can be depicted using the following equation:

$$\begin{aligned} \text{UCL} &= \bar{c} + 3\sigma \\ \text{CL} &= \bar{c} \\ \text{LCL} &= \bar{c} - 3\sigma \end{aligned} \tag{14}$$

where $\bar{c}$ is the mean value and σ is the standard deviation. They are estimated by the following equations:

$$\bar{c} = \sum_{j=1}^{m} c_j / m \tag{15}$$

$$\sigma = \sqrt{\sum_{j=1}^{m} (c_j - \bar{c})^2 / m} \tag{16}$$

Should these calculations yield a negative value for the LCL, set LCL = 0. If the number of OOL c of a surface is beyond the control line, it can be determined that the successive machining process is out of control and the leakage will occur probably in the surface of this machining process. Otherwise, the machining process of the surface should be kept. The detailed control chart can be seen in the case study section.

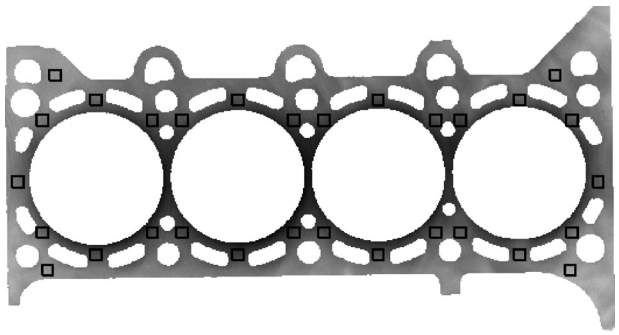

Fig. 13 The selected thirty typical regions of the top surface

3 Case Study

The proposed methodology is applied to a machining process for the top surface of vehicle engine cylinder block. The material of the engine cylinder block is cast iron FC250. This surface is a major sealing surface in automotive powertrain and it is manufactured by rough milling, semifinish milling, and finish milling. The milling process is carried out on an EX-CELL-O machining center using a face milling cutter which has a diameter of 200 mm with 15 cutting inserts intercalated by 3 wiper inserts. Quaker 370 KLG cutting fluid is used. The milling speed is 816.4 m/min, the depth of milling is 0.5 mm, and feed rate is 3360 mm/min. The machining center and cutter are shown in Fig. 11.

Leakage is always a serious concern in engine manufacturing, and it may lead to engine overheating, compression loss, and power reduction. Typically, leakage occurs most in the interface between engine cylinder block and head, and the gasket is assembled to prevent it, as seen in Fig. 12. As a consequence, the case study on the top surface of engine block cylinder is representative and significant. For example, a top surface of engine block cylinder is measured by HDM, and the converted gray image of the measured result is shown in Fig. 13. Thirty typical surface regions in the same size (6×6 mm) are selected to represent the probable leakage areas. The sampling interval is 0.2 mm, and each region has 900 points with 30×30 grid.

3.1 Finite Element Model. In order to determine the threshold of SWvc, an explicit dynamic finite element method is used to simulate the contact process in the subsection. The numerical

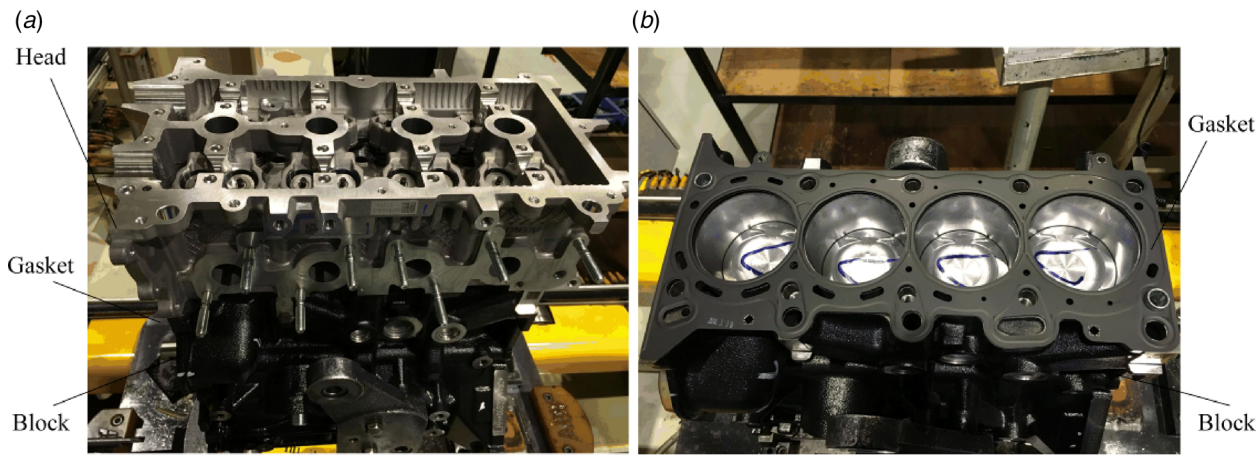

Fig. 12 (*a*) Assembled engine cylinder head and block and (*b*) gasket and block

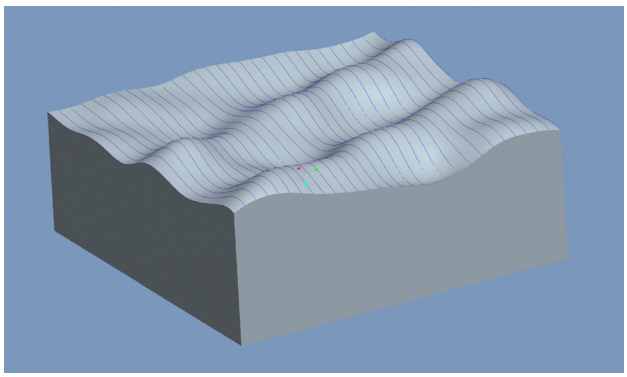

Fig. 14 Waviness surface solid

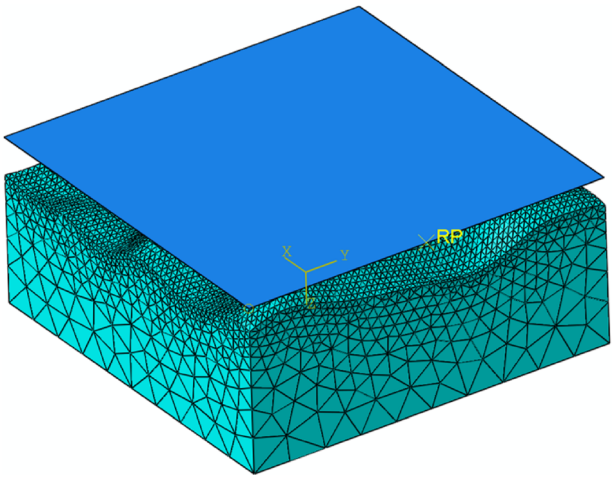

Fig. 15 Mesh generation

procedures are roughly consist of loading measured surface data, generating the solid, giving the material properties and load conditions, meshing, and determining contact deformation.

As in previous researches [41], some well-known results from contact mechanics are used to simplify the contact geometry. If there is no friction or adhesion between two rough surfaces and the surface slope is small, then elastic contact between them can be mapped to contact between a single rough surface and a rigid flat plane. Meanwhile, contact area has a well-defined thermodynamic limit, that is to say, the percentage of contact area at a given average normal pressure is independent with the system size for a fixed surface.

In this case, the gasket surface and the waviness surface of engine block cylinder both can be considered as elastic solids without friction and adhesion. Thus, a rigid flat surface is used instead of the gasket surface, and the waviness surface of engine block cylinder is considered as a three-dimensional deformable elastic rough surface. One selected 6×6 mm size waviness surface with 30×30 grid is first loaded into a computer-aided design software called PRO/ENGINEER, boundary hybrid scanning and stretching are adopted to generate the modeling waviness surface solid, see Fig. 14. Then, the solid is loaded into a computer-aided engineering software called ABAQUS for an explicit contact analysis. A same size 3D analytical rigid flat surface is generated by ABAQUS to assemble into the loaded waviness surface solid.

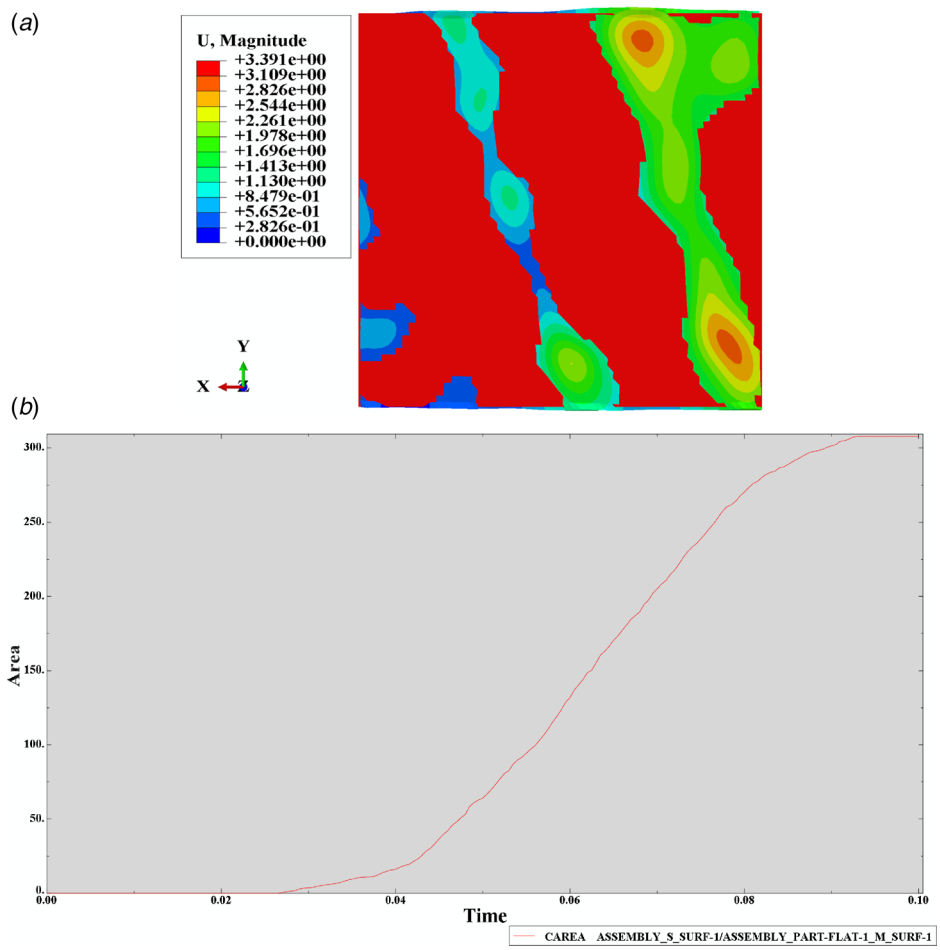

Fig. 16 (*a*) Results of displacement and (*b*) contact area

Material properties and load conditions are given according to the real work condition. The material of the waviness surface solid is cast iron FC250, and its Young's modulus, Poisson's ratio and density are 120 GPa, 0.25 and 7.0 g/cm^3, respectively. The boundary condition is that the four sides of the rigid flat surface are fixed, and simultaneously both the four sides and bottom of the waviness surface solid are fixed. The load is applied by tightened force of 10 bolts, and it is equal to about a 2 MPa face pressure. As mentioned above, numerical simulations are done for an elastic surface in contact with a rigid flat surface. A fine mesh for the elastic waviness surface is illustrated in Fig. 15. The mesh is discretized with tetrahedral elements. The mesh for the waviness surface grid contains about 11,383 nodes and 54,042 elements. By simulation, the results of displacement-deformation and contact area are illustrated in Fig. 16. As shown in Fig. 16(*a*), the maximum magnitude means the displacement of the gasket, corresponding to the noncontact area. Meanwhile, the remaining area is the contact area, and the different magnitudes represent the different displacement-deformations of the nodes in the waviness surface. Considering the face pressure is a progressively load in FEM, Fig. 16(*b*) displays the changing curves of contact area with time. It's noted that the sampling interval is 0.2 mm and the units are consistent in all directions in FEM. The final contact area is 307.6, that is $307.6 \times 0.2 \times 0.2 = 12.304$ mm, so the relative contact area is $RC = 12.304/36 \approx 0.342$. Obviously, the relative contact area of this surface region is less than 0.4, and this region is a leakage region. It can be seen more clearly in Fig. 16(*a*).

Considering the selected 30 surface probable leakage regions in Fig. 13, each surface region is analyzed by the same finite element model. At the given load, the contact area is determined for each surface region. The goal is to find out the certain surface region when the relative contact area RC is closed to 40%. Here, a small deviation of 5% is tolerated, which means that the deviations of $\pm 2.5\%$ go beyond 0.4 can be considered as 0.4. That is to say, $RC \in [0.390, 0.410]$ is equivalent to $RC \approx 0.4$. Table 1 gives the relative contact area of the thirty surface regions and the corresponding CAP, VV, and SWvoid.

In order to further clarify the relationships among these parameters, line charts and scatter diagrams are depicted to make correlation analysis and correlation coefficient r is calculated as

$$r(X,Y) = \frac{\mathrm{Cov}(X,Y)}{\sqrt{\mathrm{Var}(X)\mathrm{Var}(Y)}} \tag{17}$$

A line chart is a common chart which displays distribution information as a series of data points, and a scatter diagram indicates the potential relationship between two variables. From the definition, it is clear that VV is in direct proportion to SWvoid. Therefore, the detailed charts and diagrams of RC, CAP, and SWvoid are shown in Fig. 17, and the pairwise correlation coefficients are calculated in Table 2.

The scatter diagram indicates a strong negative correlation between RC and SWvoid, and the same to CAP and SWvoid. Meantime, RC and CAP exists a medium positive correlation. The results of correlation analysis show that determining the threshold SWvc based on the relative contact area RC is accurate and effective. Therefore, from Table 1, the relative contact area of surface region 1, 5, 8, 14, 19 are satisfied with closing to 40%. The threshold SWvc can be approximately calculated as

$$\begin{aligned} \mathrm{SWvc} \approx (&\mathrm{SWvoid}_1 + \mathrm{SWvoid}_5 + \mathrm{SWvoid}_8 + \mathrm{SWvoid}_{14} \\ &+ \mathrm{SWvoid}_{19})/5 = (0.299 + 0.303 + 0.307 + 0.293 \\ &+ 0.298)/5 = 0.300 \end{aligned} \tag{18}$$

According to contact mechanics, when the parameters such as material, process parameter and pressure change, the RC and the threshold SWvc will also change. The corresponding value of SWvc can be obtained by the proposed approach. Therefore, the threshold SWvc ≈ 0.300 is suitable for the engine cylinder block in the case study condition.

3.2 Experimental Results. As mentioned in Sec. 2.3, the normalized parameter SWvoid is independent with the area of the surface. At the same time, a strong negative correlation between RC and SWvoid is shown by the scatter diagram and the correlation coefficient. Therefore, SWvoid is selected to as the leakage indicator to report the leakage area.

From Table 1, the SWvoid of the thirty regions are calculated as $\mathrm{SWvoid}_1, \mathrm{SWvoid}_2, \ldots, \mathrm{SWvoid}_{30}$, and the threshold is SWvc = 0.3. The number of OOL c is obtained as

$$c = \sum_{i=1}^{30} k_i \tag{19}$$

$$k_i = \begin{cases} 1 & \mathrm{SWvoid}_i \geq 0.3 \\ 0 & \mathrm{SWvoid}_i < 0.3 \end{cases}, \quad i = 1, 2, \ldots, 30 \tag{20}$$

The line chart of SWvoid is depicted in Fig. 18(*a*), each selected region is determined as a leakage region by the corresponding SWvoid goes beyond 0.3. As shown in Fig. 18(*b*), the OOL leakage areas of an engine block top surface are identified. Furthermore, confirming the leakage surface and monitoring the successive machining process are achieved through the above mentioned individual control chart.

Figure 19 shows two series of successive machining process of 20 engine block top surfaces, it is clear that the first one is out of control process which exists an obvious growing tendency since the 12th block surface, and No.19 surface is very likely a leakage surface. It indicates that something changes like tool wear or chatting has probably appeared in the machining process which lead to the variation of surface topography. On the contrary, the second

Table 1 Results of surface region

Surface region	RC	CAP	VV	SWvoid
Region 1	**0.401**	0.289	10.76	**0.299**
Region 2	0.452	0.313	11.42	0.317
Region 3	0.440	0.283	10.21	0.284
Region 4	0.496	0.322	9.10	0.253
Region 5	**0.396**	0.298	10.92	**0.303**
Region 6	0.472	0.304	10.30	0.286
Region 7	0.432	0.278	13.01	0.362
Region 8	**0.391**	0.309	11.03	**0.307**
Region 9	0.504	0.343	8.52	0.237
Region 10	0.348	0.300	12.58	0.349
Region 11	0.528	0.341	8.25	0.229
Region 12	0.280	0.311	13.81	0.384
Region 13	0.434	0.331	9.86	0.274
Region 14	**0.409**	0.296	10.56	**0.293**
Region 15	0.449	0.299	10.07	0.280
Region 16	0.360	0.299	13.22	0.367
Region 17	0.457	0.338	9.34	0.260
Region 18	0.380	0.302	11.17	0.310
Region 19	**0.403**	0.330	10.72	**0.298**
Region 20	0.429	0.302	11.30	0.314
Region 21	0.480	0.341	8.90	0.247
Region 22	0.454	0.280	11.58	0.322
Region 23	0.341	0.266	12.72	0.353
Region 24	0.370	0.313	11.63	0.323
Region 25	0.478	0.342	8.89	0.247
Region 26	0.340	0.281	13.54	0.376
Region 27	0.454	0.341	9.40	0.261
Region 28	0.500	0.308	10.16	0.282
Region 29	0.480	0.302	9.76	0.271
Region 30	0.420	0.309	10.38	0.288

Note: In Table 1, The values of RC in bold are considered as closing to 0.4, and the values of SWvoid in bold are the corresponding to RC in the same surface region.

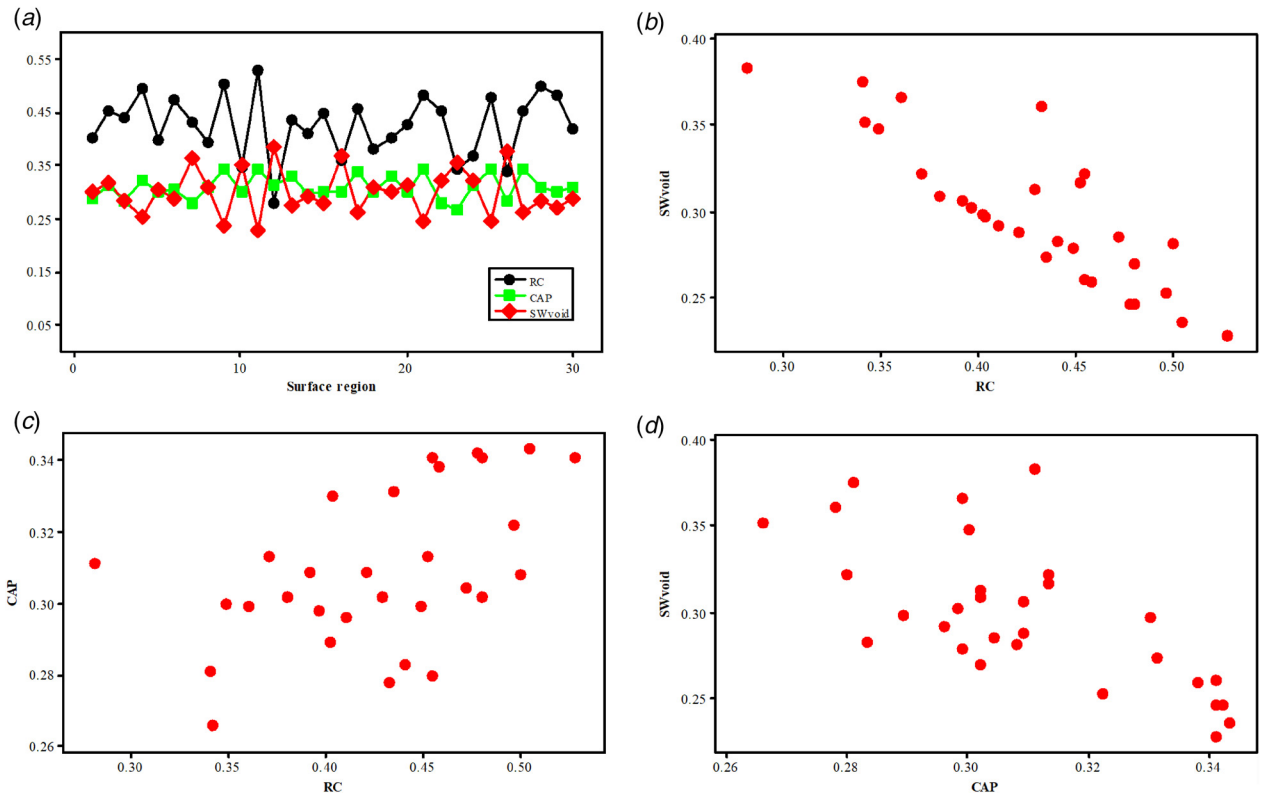

Fig. 17 (*a*) Line charts of RC, CAP, and SWvoid, (*b*) scatter diagram of RC and SWvoid, (*c*) scatter diagram of RC and CAP, and (*d*) scatter diagram of CAP and SWvoid

Table 2 Correlation coefficient

Correlation coefficient	r(RC, SWvoid)	r(RC, CAP)	r(CAP, SWvoid)
r	−0.851	0.493	−0.702

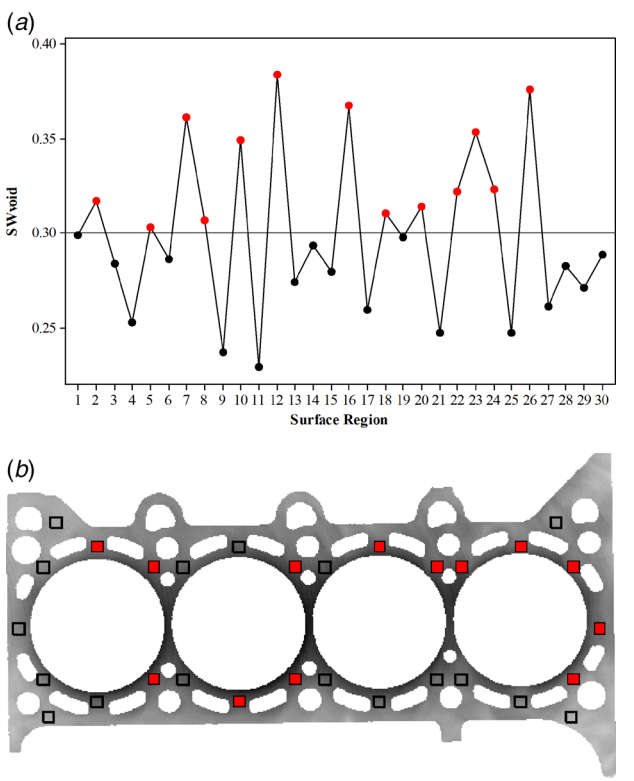

Fig. 18 (*a*) The line chart of SWvoid and (*b*) OOL leakage regions

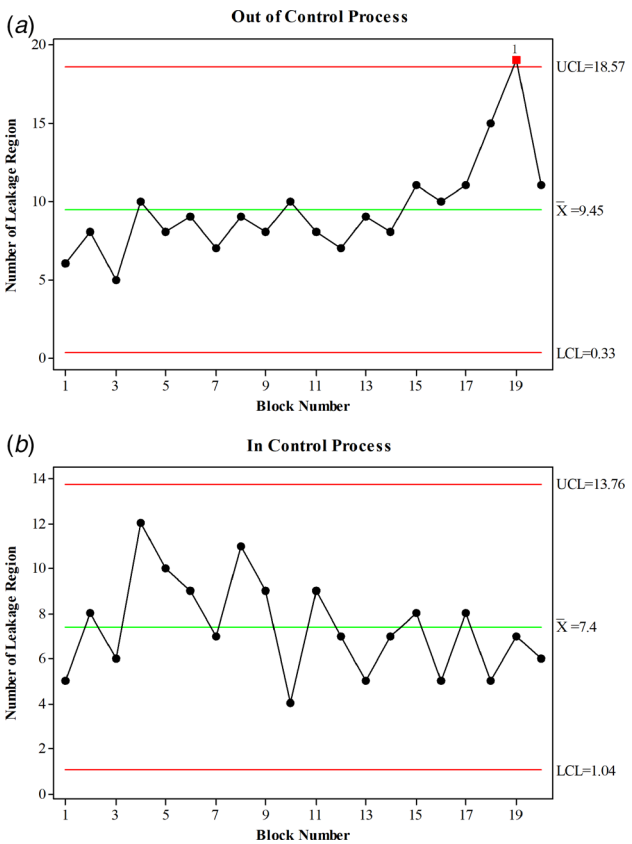

Fig. 19 (*a*) Out of control process and (*b*) in control process

machining process is relatively stable and the probability of leakage surfaces is small.

The control chart for leakage monitoring enables leakage susceptibility mensuration long before pressure test, and detects more leak-prone parts which have been machined. At the same time, the leakage potential surface can be prevented entering the next costly procedure in time from the control chart. Furthermore, leakage monitoring ensures a higher quality product that will incur lower postdelivery warranty costs and higher customer satisfaction.

4 Conclusions

This paper presents a leakage monitoring method in static seal interface using 3D surface topography as indicators. To achieve this functional analysis, a combination of spline filter and morphological filter are employed. The 3D surface topography indicators including leakage parameters CAP, VV, and SWvoid are calculated by virtual gasket surface $SC(x, y)$ and waviness surface $SW(x, y)$. According to Persson contact mechanics and percolation theory, the threshold of leakage parameter is confirmed using FEM simulation. Then, an individual control chart is proposed to monitor the leakage surface of the successive machining process. Experimental results indicate that the proposed monitoring method is valid to precontrol the machining process and prevent leakage occurring.

Furthermore, there have been only a few attempts on leakage monitoring, the proposed approach is a first idea to account for this kind of problems. Thus, there is a large amount of room for important improvements. Moreover, in order to enhance quality control, the quantitative leakage rate experimental investigation will be designed to further reveal and test the potential relationship between leakage and surface topography, which is the next research topic in future.

Acknowledgment

All experiments are performed at SAIC GM Wuling Automobile (SGMW), and we are grateful to SGMW engineers for their experimental support.

Funding Data

- National Natural Science Foundation of China (Grant Nos. 51535007 and 51775343).

References

[1] Flitney, R. K., 2011, *Seals and Sealing Handbook*, Elsevier, Oxford, UK.
[2] Persson, B. N. J., and Yang, C., 2008, "Theory of the Leak-Rate of Seals," J. Phys.: Condens. Matter, **20**(31), p. 315011.
[3] Aharony, A., and Stauffer, D., 2003, *Introduction to Percolation Theory*, Taylor & Francis, London.
[4] Persson, B. N. J., Albohr, O., Creton, C., and Peveri, V., 2004, "Contact Area Between a Viscoelastic Solid and a Hard, Randomly Rough, Substrate," J. Chem. Phys., **120**(18), pp. 8779–8793.
[5] Lorenz, B., and Persson, B. N. J., 2009, "Leak Rate of Seals: Comparison of Theory With Experiment," Europhys. Lett., **86**(4), p. 44006.
[6] Lorenz, B., and Persson, B. N. J., 2010, "Leak Rate of Seals: Effective-Medium Theory and Comparison With Experiment," Eur. Phys. J. E, **31**(2), pp. 159–167.
[7] Bottiglione, F., Carbone, G., Mangialardi, L., and Mantriota, G., 2009, "Leakage Mechanism in Flat Seals," J. Appl. Phys., **106**(10), p. 104902.
[8] Bottiglione, F., Carbone, G., and Mantriota, G., 2009, "Fluid Leakage in Seals: An Approach Based on Percolation Theory," Tribol. Int., **42**(5), pp. 731–737.
[9] Marie, C., and Lasseux, D., 2007, "Experimental Leak-Rate Measurement Through a Static Metal Seal," ASME J. Fluids Eng., **129**(6), pp. 799–805.
[10] Robbe-Valloire, F., and Prat, M., 2008, "A Model for Face-Turned Surface Microgeometry. Application to the Analysis of Metallic Static Seals," Wear, **264**(11–12), pp. 980–989.
[11] Okada, H., Itoh, T., and Suga, T., 2008, "The Influence of Surface Profiles on Leakage in Room Temperature Seal-Bonding," Sens. Actuators, A, **144**(1), pp. 124–129.
[12] Haruyama, S., Nurhadiyanto, D., Choiron, M. A., and Kaminishi, K., 2013, "Influence of Surface Roughness on Leakage of New Metal Gasket," Int. J. Pressure Vessels Piping, **111–112**, pp. 146–154.
[13] Marie, C., Lasseux, D., Zahouani, H., and Sainsot, P., 2003, "An Integrated Approach to Characterize Liquid Leakage Through Metal Contact Seal," Eur. J. Mech. Environ. Eng., **48**(2), pp. 81–86.
[14] Ledoux, Y., Lasseux, D., Favreliere, H., Samper, S., and Grandjean, J., 2011, "On the Dependence of Static Flat Seal Efficiency to Surface Defects," Int. J. Pressure Vessels Piping, **88**(11–12), pp. 518–529.
[15] Malburg, M. C., 2003, "Surface Profile Analysis for Conformable Interfaces," ASME J. Manuf. Sci. Eng., **125**(3), pp. 624–627.
[16] Liao, Y., Stephenson, D. A., and Ni, J., 2012, "Multiple-Scale Wavelet Decomposition, 3D Surface Feature Exaction and Applications," ASME J. Manuf. Sci. Eng., **134**(1), p. 011005.
[17] Ren, J., Park, C., and Wang, H., 2018, "Stochastic Modeling and Diagnosis of Leak Areas for Surface Assembly," ASME J. Manuf. Sci. Eng., **140**(4), p. 041011.
[18] Arghavani, J., Derenne, M., and Marchand, L., 2002, "Prediction of Gasket Leakage Rate and Sealing Performance Through Fuzzy Logic," Int. J. Adv. Manuf. Technol., **20**(8), pp. 612–620.
[19] Xin, L., and Gaoliang, P., 2016, "Research on Leakage Prediction Calculation Method for Static Seal Ring in Underground Equipments," J. Mech. Sci. Technol., **30**(6), pp. 2635–2641.
[20] Huang, Z., Shih, A. J., and Ni, J., 2006, "Laser Interferometry Hologram Registration for Three-Dimensional Precision Measurements," ASME J. Manuf. Sci. Eng., **128**(4), pp. 1006–1013.
[21] Wang, M., Xi, L., and Du, S., 2014, "3D Surface Form Error Evaluation Using High Definition Metrology," Precis. Eng., **38**(1), pp. 230–236.
[22] Du, S., and Fei, L., 2015, "Co-Kriging Method for Form Error Estimation Incorporating Condition Variable Measurements," ASME J. Manuf. Sci. Eng., **138**(4), p. 041003.
[23] Du, S., Liu, C., and Huang, D., 2015, "A Shearlet-Based Separation Method of 3D Engineering Surface Using High Definition Metrology," Precis. Eng., **40**, pp. 55–73.
[24] Wang, M., Shao, Y., Du, S., and Xi, L., 2015, "A Diffusion Filter for Discontinuous Surface Measured by High Definition Metrology," Int. J. Precis. Eng. Manuf., **16**(10), pp. 2057–2062.
[25] Du, S., Liu, T., Huang, D., and Li, G., 2018, "A Fast and Adaptive Bi-Dimensional Empirical Mode Decomposition Approach for Filtering of Workpiece Surfaces Using High Definition Metrology," J. Manuf. Syst., **46**, pp. 247–263.
[26] Du, S., Liu, C., and Xi, L., 2014, "A Selective Multiclass Support Vector Machine Ensemble Classifier for Engineering Surface Classification Using High Definition Metrology," ASME J. Manuf. Sci. Eng., **137**(1), p. 011003.
[27] Huang, D., Du, S., Li, G., and Wu, Z., 2017, "A Systematic Approach for Online Minimizing Volume Difference of Multiple Chambers in Machining Processes Based on High-Definition Metrology," ASME J. Manuf. Sci. Eng., **139**(8), p. 081003.
[28] Shao, Y., Du, S., and Xi, L., "3D Machined Surface Topography Forecasting With Space-Time Multioutput Support Vector Regression Using High Definition Metrology," 37th Computers and Information in Engineering Conference, Vol. 1, p. V001T002A069.
[29] Wang, M., Ken, T., Du, S., and Xi, L., 2015, "Tool Wear Monitoring of Wiper Inserts in Multi-Insert Face Milling Using Three-Dimensional Surface Form Indicators," ASME J. Manuf. Sci. Eng., **137**(3), p. 031006.
[30] ISO, 2015, "Geometrical Product Specifications (GPS)-Filtration—Part 22: Linear Profile Filters: Spline Filter," International Organization for Standardization, Geneva, Switzerland, Standard No. ISO 16610-22:2015.
[31] ISO, 2015, "Geometrical Product Specifications (GPS)-Filtration—Part 1: Overview and Basic Concepts," International Organization for Standardization, Geneva, Switzerland, Standard No. ISO 16610-1:2015.
[32] Krystek, M., 1996, "Form Filtering by Splines," Measurement, **18**(1), pp. 9–15.
[33] Maragos, P., and Schafer, R., 1987, "Morphological Filters—Part I: Their Set-Theoretic Analysis and Relations to Linear Shift-Invariant Filters," IEEE Trans. Acoust., Speech, Signal Process., **35**(8), pp. 1153–1169.
[34] ISO, 2015, "Geometrical Product Specifications (GPS)-Filtration—Part 40: Morphological Profile Filters: Basic Concepts," International Organization for Standardization, Geneva, Switzerland, Standard No. ISO 16610-40:2015.
[35] ISO, 2015, "Geometrical Product Specifications (GPS)-Filtration—Part 41: Morphological Profile Filters: Disk and Horizontal Line-Segment Filters," International Organization for Standardization, Geneva, Switzerland, Standard No. ISO 16610-41:2015.
[36] ISO, 2015, "Geometrical Product Specifications (GPS)-Filtration—Part 85: Morphological Areal Filters: Segmentation," International Organization for Standardization, Geneva, Switzerland, Standard No. ISO 16610-85:2015.
[37] ISO, 2012, "Geometrical Product Specifications (GPS)-Surface Texture: Areal—Part 2: Terms, Definitions and Surface Texture Parameters," International Organization for Standardization, Geneva, Switzerland, Standard No. ISO 25178-2:2012.
[38] ISO, 1997, "Geometrical Product Specifications (GPS)-Surface Texture: Profile Method: Terms, Definitions and Surface Texture Parameters," International Organization for Standardization, Geneva, Switzerland, Standard No. ISO 4287:1997.
[39] Hyun, S., Pel, L., Molinari, J. F., and Robbins, M. O., 2004, "Finite-Element Analysis of Contact Between Elastic Self-Affine Surfaces," Phys. Rev. E: Stat., Nonlinear, Soft Matter Phys., **70**(2 Pt 2), p. 026117.
[40] Megalingam, A., and Mayuram, M. M., 2012, "Comparative Contact Analysis Study of Finite Element Method Based Deterministic, Simplified Multi-Asperity and Modified Statistical Contact Models," ASME J. Tribol., **134**(1), p. 014503.
[41] Johnson, K. L., 1985, *Contact Mechanics*, Cambridge University Press, New York.